I&EC research
Industrial & Engineering Chemistry Research

Article

pubs.acs.org/IECR

Ultrafiltration Membranes Enhanced with Electrospun Nanofibers Exhibit Improved Flux and Fouling Resistance

Kerianne M. Dobosz, Christopher A. Kuo-Leblanc, Tyler J. Martin, and Jessica D. Schiffman*

Department of Chemical Engineering University of Massachusetts Amherst, Amherst, Massachusetts 01003-9303, United States

Supporting Information

ABSTRACT: In this study, we have improved membrane performance by enhancing ultrafiltration membranes with electrospun nanofibers. The high-porosity nanofiber layer provides a tailorable platform that does not affect the base membrane structure. To decouple the effects that nanofiber chemistry and morphology have on membrane performance, two polymers commonly used in the membrane industry, cellulose and polysulfone, were electrospun into a layer that was 50 μm thick and consisted of randomly accumulated 1-μm-diameter fibers. Fouling resistance was improved and selectivity was retained by ultrafiltration membranes enhanced with a layer of either cellulose or polysulfone nanofibers. Potentially because of their better mechanical integrity, the polysulfone nanofiber-membranes demonstrated a higher pure-water permeance across a greater range of transmembrane pressures than the cellulose nanofiber-membranes and control membranes. This work demonstrates that nanofiber-enhanced membranes hold potential as versatile materials platforms for improving the performance of ultrafiltration membranes.

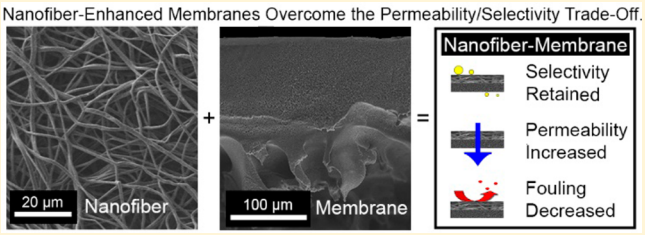

1. INTRODUCTION

Ultrafiltration is a membrane-based process used in many industrial processes where high separation efficiency is required, including water purification, biological filtration, and beverage clarification. Ideally, the structure of an ultrafiltration membrane should have a high porosity, a narrow pore distribution, and a thin skin layer.[1] Additionally, hydrophilicity endows an ultrafiltration membrane with excellent wettability, which improves water permeation and delays the development of fouling. To improve membrane performance, previous research has explored two major modification strategies. Specifically, researchers have modified the surface of the membrane, or they have integrated molecules into the body of the membrane. Membranes coated with hydrophilic polymers, reactive nanomaterials, or nanotopographic features offer a number of advantages over their mixed-matrix counterparts, such as concentrating the active material at the surface of the membrane and tailoring an already optimized ultrafiltration membrane.[2−8] Unfortunately, surface modifications that effectively advance one property, for example, increasing the flux of the membrane, often impede a different property, such as selectivity.[9−11] Therefore, a different approach that alters ultrafiltration membranes without adversely impacting their flux or selectivity is needed.

Electrospinning is a commercially viable[12] fabrication technique that enables the large-scale production of nanofiber mats with macroscale interstitial spaces and porosity values greater than 80%.[13] Typically, the produced fiber mats comprise randomly accumulated nanoscale- or microscale-diameter fibers with large surface-to-volume ratios and high specific surface areas. Fiber mats from over 100 different synthetic and natural polymers have been electrospun. Because of their unique structural and chemical characteristics, free-standing electrospun nanofiber mats have been used as prefilters or as microfiltration membranes in water, air, and pharmaceutical separations.[14−18]

In addition, nanofibers have been incorporated into the bodies of membranes to improve an aspect of membrane performance. Hoover et al.[19] used electrospun nanofibers as a support layer for forward-osmosis membranes with enhanced mechanical robustness. Titanium dioxide fibers[20] and polyaniline nanofibers[21] incorporated into the bodies of ultrafiltration membranes improved the hydrophilicity and flux but increased the pore size by ∼50%, thus altering membrane selectivity. Polyurethane nanofibers coated with silver nanoparticles successfully increased the biocidal properties of ultrafiltration membranes but reduced the permeability by 35%.[22,23] The aim of this work was to determine whether adding a highly porous nonselective layer of continuous nanofibers directly onto the surface of an ultrafiltration membrane can improve its permeability or fouling resistance without adversely affecting its molecular-weight cutoff. In this work, the nanofiber layers are not acting as prefilters, nor are we placing two membranes in series; rather, we are preparing composite ultrafiltration membranes with a nanofiber layer physically pressed to the surface of the membrane.

Received: February 13, 2017
Revised: April 20, 2017
Accepted: April 25, 2017
Published: April 25, 2017

DOI: 10.1021/acs.iecr.7b00631
Ind. Eng. Chem. Res. 2017, 56, 5724−5733

Here, we report the creation of composite ultrafiltration membranes with a high-porosity nanofiber layer. Cellulose and polysulfone, two polymers commonly used in the membrane industry,[24] were electrospun to decouple the effects that nanofiber hydrophilicity and morphology have on ultrafiltration membrane performance. Cellulose is the most abundant natural polymer; it is hydrophilic and can easily undergo further chemical modifications.[25,26] Polysulfone is a hydrophobic polymer with high chemical and mechanical robustness.[27] The selectivity, pure-water flux, and fouling resistance of well-characterized ultrafiltration membranes enhanced with a cellulose or polysulfone nanofiber layer were evaluated.

2. EXPERIMENTAL SECTION

2.1. Materials and Chemicals. All compounds were used as received. Polysulfone (M_n = 22000 Da), cellulose acetate (M_n = 30000 Da), *N*,*N*-dimethylformamide (DMF, anhydrous, 99.8%), tetrahydrofuran (THF, containing 250 ppm butylated hydroxytoluene as an inhibitor, ACS reagent, ≥99.0%), bovine serum albumin (BSA, heat-shock fraction, >98%), and Bradford reagent (for 1−1400 μg of protein/mL) were purchased from Sigma-Aldrich (St. Louis, MO). Acetone (histological grade), sodium hydroxide, ethanol (absolute anhydrous), and isopropyl alcohol (Certified ACS Plus) were purchased from Fisher Scientific (Pittsburgh, PA). Polyethylene glycol (PEG, M_n = 4, 10, 35, 55, 95, 150, and 203 kDa) was purchased from Polymer Source (Montreal, Quebec, Canada). Deionized (DI) water was obtained from a Barnstead Nanopure Infinity water purification system (Thermo Fisher Scientific, Waltham, MA).

2.2. Electrospinning of Cellulose and Polysulfone Nanofibers. Solutions consisting of 15 wt % cellulose acetate in acetone[28] and 21 wt % polysulfone in THF/DMF (1:1 wt/wt) were mixed for 24 h at 20 rpm using an Arma-Rotator A-1 apparatus (Elmeco Engineering, Rockville, MD). A cellulose acetate or polysulfone solution was loaded into a 5 mL Luer-Lock tip syringe capped with a Precision Glide 18-gauge or 22-gauge needle (Becton, Dickinson & Company, Franklin Lakes, NJ), respectively, after which the syringe was secured to an infusion syringe pump (Cole Parmer, Vernon Hills, IL). Alligator clips were used to connect the electrode of a high-voltage supply (Gamma High Voltage Research, Ormond Beach, FL) to the needle and the electrode of a copper plate (152.4 mm × 152.4 mm × 3.2 mm, McMaster-Carr, Robbinsville, NJ). The copper plate was wrapped in aluminum foil and held at a fixed separation distance of 10 cm. Constant feed rates of 3 and 2 mL h^{-1} and applied voltages of 25 and 17 kV were used to electrospin the cellulose acetate and polysulfone solutions, respectively. The assembled electrospinning apparatus was housed in a custom-built environmental chamber equipped with a desiccant unit (Drierite, Xenia, OH) that maintained the temperature at 22 ± 1 °C and the relative humidity at 55% and 23% during the electrospinning of cellulose acetate and polysulfone, respectively. To generate nanofiber layers with a consistent bulk thickness, cellulose acetate was electrospun for 1 h, and polysulfone was electrospun for 0.33 h. After being peeled off the collector plate, the cellulose acetate and polysulfone nanofiber layers were sandwiched between Teflon sheets (3.2 mm × 101.6 mm × 152.4 mm, McMaster-Carr) and placed in a furnace for 1 h at 208 and 165 °C, respectively. To generate cellulose nanofibers, the heat-treated cellulose acetate nanofibers were submerged in a 0.1 M sodium hydroxide DI water/ethanol solution (4:1 v/v) for 14 h before being washed three times with DI water.[29] All nanofiber layers were stored in a desiccator at room temperature (23 °C) until use.

2.3. Assembly of Cellulose Nanofiber-Membranes and Polysulfone Nanofiber-Membranes. Biomax poly(ether sulfone) ultrafiltration membranes from EMD Millipore (Billerica, MA) with a reported nominal molecular-weight limit of 100 kDa were used as the base membranes. To create ultrafiltration membranes enhanced with cellulose or polysulfone nanofibers, a layering technique was used to create a membrane consisting of a nanofiber layer on top of a commercial membrane. The nanofiber layer was placed on the surface of the membrane. No additional adhesives or forces were used. Internal O-rings in the dead-end and cross-flow testing cells held the nanofiber layers to the membranes to form the composite membranes tested in this study. Throughout this article, the assembled ultrafiltration membranes functionalized with a cellulose nanofiber or a polysulfone nanofiber layer are referred to as cellulose nanofiber-membranes and polysulfone nanofiber-membranes, respectively. Control membranes are ultrafiltration membranes without a nanofiber layer.

2.4. Materials Characterization. Nanofiber chemistry was confirmed using Fourier transform infrared (FTIR) spectroscopy (Bruker Alpha, Bruker Optics, Billerica, MA). Micrographs of nanofibers and membrane cross sections were acquired using an EVO50 scanning electron microscope (SEM, Carl Zeiss Inc., Thornwood, NY). Samples were coated with an XE200 xenon magnetron sputter coater (Edwards Vacuum, Albany, NY) for 30 s. Nanofiber diameter distributions were determined using *ImageJ* 1.47 software (National Institutes of Health, Bethesda, MD) by measuring 50 random fibers from five micrographs. SEM micrographs were obtained after the fabric support layer was removed from the commercial ultrafiltration membrane, the membrane or nanofiber-enhanced membrane was submerged in liquid nitrogen, and the sample was cracked.[30] Higher-resolution micrographs of membrane pores were acquired using a Magellan 400 XHR scanning electron microscope (FEI, Hillsboro, OR). Membranes were sputter coated for 40 s with platinum before SEM imaging (Cressington 208 HR, Cressington Scientific Instruments, Watford, U.K.). Using *ImageJ*, a total of 100 pore measurements from five separate membrane samples were taken to determine the average membrane pore diameter. Pore coverage was determined using *ImageJ* by analyzing SEM micrographs by means of the threshold and particle analysis functions. The bulk (*z*-axis) thicknesses of nanofiber layers and membranes were measured at five different locations on five separate samples using a Mitutoyo 293-330 digital micrometer (Toronto, Ontario, Canada). Contact angle measurements using 5 μL drops of DI water were carried out using a home-built apparatus equipped with a Nikon D5100 digital camera with a 60-mm lens and 68-mm extension tube (Nikon, Melville, NY).[31] The contact angles reported are the averages of 25 drops on five different nanofiber layers and membrane samples.

2.5. Performance of Cellulose Nanofiber-Membranes and Polysulfone Nanofiber-Membranes. Size selectivity or molecular-weight cutoff (MWCO) analysis was conducted on the cellulose nanofiber-membranes, polysulfone nanofiber-membranes, and control membranes.[32] PEG was used as a model molecule because of its high solubility in water, limited fouling, and wide range of available molecular weights. Nanofiber layers (25-mm circles) were prewet by being submerged in DI water for 12 h prior to testing. Base ultrafiltration membranes (25-mm circles) were immersed in 20

DOI: 10.1021/acs.iecr.7b00631
Ind. Eng. Chem. Res. 2017, 56, 5724−5733

mL of isopropyl alcohol for 0.5 h before being flushed to remove glycerol (a preservation substance) and compacted for 1 h with DI water using a 10 mL dead-end stirred cell at an applied pressure of 1 bar (Sterlitech, Kent, WA). In the dead-end stirred cell, cellulose nanofiber-membranes, polysulfone nanofiber-membranes, and control membranes were challenged with 10 g of a PEG feed solution (500 mg L^{-1}) using an applied pressure of 2 bar and a stir rate of 600 rpm. Individual PEG solutions were prepared with different molecular weights of PEG, including 4, 35, 55, 95, 150, and 203 kg mol^{-1}. The mass of the permeate was monitored over time, and the concentration (C) of PEG was compared to a standard curve using a high-performance liquid chromatography (HPLC) instrument (LC-20AT Shimadzu, Marlborough, MA) with a refractive index detector (RID-10A, Shimadzu).[33] The PEG rejection values were calculated according to the equation[34]

$$\text{rejection (\%)} = \left(1 - \frac{C_{\text{permeate}}}{C_{\text{feed}}}\right) \times 100 \quad (1)$$

where C_{permeate} is the final concentration of PEG in the permeate and C_{feed} is the concentration of PEG in the initial feed solution. Experiments were conducted in triplicate. By definition, the MWCO of a membrane is the lowest molecular weight of PEG at which the membrane exhibits a rejection of ~90%.

The pure-water flux of free-standing nanofiber layers (no support membrane) and control membranes (25-mm circles) were determined using the dead-end stirred cell, consistent with a previously reported method.[35,36] Here, 4 L of DI water was loaded into a pressure vessel at an applied pressure of 0.14 bar and a stir rate of 600 rpm. A spacer with an inner diameter of 8 mm restricted the membrane active area to 201 mm^2. For each test, membrane compaction was assumed when the change in flux was less than 5% from the previous time point. The permeate stream was massed every 5 min using a scale connected to serial port monitor (Eltima, Frankfurt, Germany). The pure-water flux, was calculated using the equation

$$\text{pure-water flux}\left(\frac{\text{L}}{\text{m}^2\,\text{h}}\right) = \frac{V_{\text{water}}}{A_{\text{membrane}}\Delta t} \quad (2)$$

where V_{water} is the volume of water that permeated through the membrane, A_{membrane} is the geometric area of the membrane operating in the flow cell, and Δt is the change in time.

The pure-water flux of the cellulose nanofiber-membranes, polysulfone nanofiber-membranes, and control membranes were evaluated using a custom-build cross-flow cell (channel dimensions of 28 mm long, 17 mm wide, and 1.5 mm deep) equipped with a 31 mil low-foulant spacer and a permeate carrier (Sterlitech). All tests were conducted in cross-flow at a flow rate of 50 mL min^{-1} enabled by a reciprocating pump (Eldex, Napa, CA) followed by a dampener (Cat Pumps, Minneapolis, MN).[37−40] An ultrafiltration membrane (29 mm × 45 mm) was placed with its active side facing down into the cross-flow cell and flushed at a transmembrane pressure (TMP) of 1.5 bar, where it was held for 1 min to remove glycerol (a preservation substance) as confirmed by HPLC. Next, the cross-flow cell was completely disassembled to load a prewetted cellulose or polysulfone nanofiber layer (29 mm × 45 mm × 0.051 mm) below the flushed ultrafiltration membrane before pressure was applied at the desired TMP, which was calculated using the following equation:

$$\text{TMP (bar)} = \frac{P_{\text{feed}} - P_{\text{retentate}}}{2} - P_{\text{permeate}} \quad (3)$$

where P_{feed} is the pressure of the feed stream at the inlet of the flow cell, $P_{\text{retentate}}$ is the pressure of the retentate stream, and P_{permeate} is the pressure of the permeate stream. Cross-flow velocities of 36 and 35 m s^{-1} were experienced by the control membranes and the nanofiber-enhanced membranes, respectively. Pure-water flux was evaluated as previously described for an active area of 5.44 cm^2. The hydraulic permeance or total membrane throughput as a function of TMP was determined using the equation[41]

$$\text{hydraulic permeance}\left(\frac{\text{L}}{\text{m}^2\,\text{h bar}}\right) = \frac{\text{pure-water flux}}{\text{TMP}} \quad (4)$$

with the compacted flux data for TMPs ranging from 0.5 to 4.5 bar acquired in triplicate.

2.6. Fouling Resistance of Cellulose Nanofiber-Membranes and Polysulfone Nanofiber-Membranes. The model protein BSA was used in membrane fouling experiments. Cellulose nanofiber-membranes, polysulfone nanofiber-membranes, and control membranes were challenged with a feed of 10 g of BSA solution prepared at a concentration of 250 mg L^{-1} (pH 4.55) using a dead-end stirred cell at an applied pressure of 1 bar.[42,35,36] The time required for 10 g of BSA solution to pass through the membrane was recorded. The permeate was collected, and the BSA concentration was determined using a Bradford reagent and an absorbance microplate reader (BioTek ELx800, Winooski, VT) at an absorbance of 600 nm.[43] A calibration curve was used to convert the microplate readings into protein concentration.

To determine the fouling of cellulose nanofibers and polysulfone nanofibers exposed to BSA for longer times, 1-h batch adsorption tests were conducted. Cellulose and polysulfone nanofiber layers (1 cm × 1 cm) were placed into BSA solution (1.25 mL) at a concentration of 250 g L^{-1} (pH 4.55) and agitated at 100 rpm. The amount of BSA that adsorbed onto the nanofiber layer was determined from the final concentration of BSA in the solution, as described previously. Experiments were conducted in triplicate.

2.7. Statistics. To calculate hydraulic permeance values from the pure-water flux data, a linear regression that accounted for the error from each individual data point was employed. The statistical significance of the linear regressions was evaluated using a modified z-test.[44] For all other data, statistical significant differences between samples were determined using an unpaired Student's t test with a p value of 0.05.

3. RESULTS AND DISCUSSION

3.1. Characteristics of Cellulose Nanofibers and Polysulfone Nanofibers. To the best of our knowledge, the effects of adding continuous electrospun nanofibers onto the surface of ultrafiltration membranes have not yet been demonstrated. To decouple the role of the fibrous morphology from that of the nanofiber chemistry/hydrophilicity, we synthesized nanofibers with chemistries common in membrane technology. Cellulose and polysulfone nanofibers with the same morphology, statistically equivalent nanofiber diameter, and equivalent bulk thickness were synthesized (Figures 1 and S1). To produce cellulose nanofibers, cellulose acetate was electrospun and converted to cellulose by an alkaline treatment. Figure 1 shows that randomly accumulated cellulose nanofibers with a continuous and cylindrical morphology were fabricated. The

DOI: 10.1021/acs.iecr.7b00631
Ind. Eng. Chem. Res. 2017, 56, 5724−5733

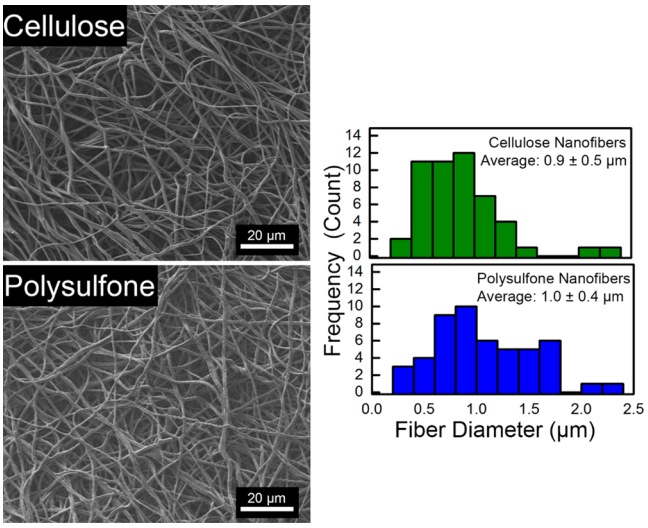

Figure 1. SEM micrographs of electrospun cellulose and polysulfone nanofibers. Also displayed are the fiber diameter distributions for the cellulose and polysulfone nanofibers, along with the average fiber diameters and standard deviations. The average fiber diameters of the cellulose and polysulfone nanofibers were statistically equivalent.

cellulose nanofibers had an average diameter of 0.9 ± 0.5 μm, consistent with previous work.[43] The FTIR spectra of the as-spun cellulose acetate and the cellulose nanofibers indicate, by the disappearance of the 1750 cm^{-1} peak,[45] that the acetate groups were replaced with hydroxyl groups (Figure S2 of the Supporting Information).

Polysulfone nanofibers with a smooth cylindrical morphology and, for the first time, an average fiber diameter of 1.0 ± 0.4 μm, were successfully electrospun (Figure 1). Previous works have involved the electrospinning of smaller-diameter polysulfone nanofibers (0.15−0.50 μm) using DMF or dimethylacetamide as the solvent.[16,46−48] To electrospin polysulfone nanofibers with the same fiber diameter as the cellulose nanofibers, we systematically investigated alterations of the previously reported electrospinning process. Successful parameter changes included increasing the electrospinning precursor polymer concentration and employing a mixed solvent system featuring THF, a high-volatility solvent. FTIR spectra of the polysulfone nanofibers (Figure S2) confirm the presence of characteristic polysulfone peaks, including the aromatic C—H bond stretch at 2966 cm^{-1}, the S═O asymmetric stretch at 1294 cm^{-1}, and the CO—C stretch at 1236 cm^{-2}.[5] The C—N vibration of DMF at 644 cm^{-1} and the "breathing" ring mode of THF at 900 cm^{-1} were not present in the FTIR spectra, indicating that the solvents had evaporated from the fibers during the electrospinning process.[49]

The water contact angle measurement for the cellulose nanofiber layer was 0°, consistent with the literature report that this material is hydrophilic.[50] The polysulfone nanofibers had a water contact angle of 110 ± 5°, indicative of hydrophobicity. Contact angle measurements are influenced by both the chemistry and the structure of a material, that is, a flat film often has a different contact angle than a nanofiber layer. A previous study reported the contact angle of polysulfone films to be 85°,[51] whereas polysulfone nanofibers with a diameter of ∼0.47 μm were found to exhibit a higher contact angle of 140°,[16] which is similar to the value that we measured. Thus, flexible nanofiber layers with different chemistries (cellulose and polysulfone) and hydrophilicities (hydrophilic and hydrophobic) but equivalent average diameters, bulk thicknesses, and morphologies were electrospun; next, we explored the structure−property relationships of the nanofiber-enhanced membranes.

3.2. Characteristics of Cellulose Nanofiber-Membranes and Polysulfone Nanofiber-Membranes. The electrospinning time was optimized so that the bulk thicknesses of the cellulose and polysulfone nanofiber layers, which were pressed onto the surface of the ultrafiltration membranes, would be statistically equivalent, at 50 ± 10 and 48 ± 10 μm, respectively. Nanofiber layers with a thickness of 50 μm were chosen because thinner layers (∼20 μm) did not withstand the preliminary compaction tests that we conducted (Figure S3). There was no improvement in pure-water flux if a nanofiber layer is too thick (e.g., ∼125 μm). Thus, based on our preliminary experiments, we selected to move forward by focusing on nanofiber layers that were ∼50 μm thick, as they were the thinnest nanofiber layers that we could consistently electrospin from both polymers that also demonstrated an increase in the pure-water flux.

Cross-sectional micrographs of the control membranes, cellulose nanofiber-membranes, and polysulfone nanofiber-membranes are shown in Figure 2. It should be noted that

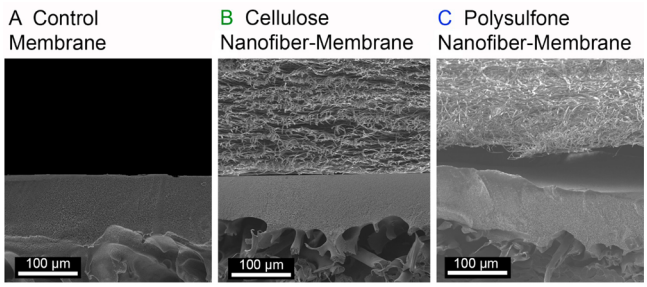

Figure 2. SEM micrographs displaying representative cross sections of a control membrane, a cellulose nanofiber-membrane, and a polysulfone nanofiber-membrane.

the observed gap between the polysulfone nanofiber layer and the ultrafiltration membrane is an artifact of the liquid-nitrogen sample preparation needed for acquiring cross-sectional SEM micrographs; the gap is consistent with previous reports.[19] The control membranes had a sponge-like morphology[52] and an average surface pore diameter of 18.0 ± 8 nm that covered 6.5 ± 0.3% of the membrane surface. The control membranes had an overall thickness of 103 ± 4 μm, as measured using a digital micrometer that provides very accurate measurements. Upon functionalization of the membranes with an electrospun nanofiber layer, the membrane thickness increased to 150 ± 18 and 150 ± 19 μm for the cellulose nanofiber-membranes and polysulfone nanofiber-membranes, respectively.

The hydrophilicity of the membranes was determined using water contact angle measurements. The control membranes had a contact angle of 41 ± 20°, consistent with literature on poly(ether sulfone) membranes.[40] Because of the hydrophilic properties of the cellulose nanofiber layer, the cellulose nanofiber-membranes exhibited an increased hydrophilicity of 0°. The polysulfone nanofiber layer also dictated the water contact angle of the polysulfone nanofiber-membranes; it was 120 ± 0°. The addition of the nanofiber layer altered the contact angle of the nanofiber-enhanced membranes, making

DOI: 10.1021/acs.iecr.7b00631
Ind. Eng. Chem. Res. 2017, 56, 5724−5733

them statistically different from those of the control membranes.

3.3. Selectivity of Cellulose Nanofiber-Membranes and Polysulfone Nanofiber-Membranes. The cellulose and polysulfone nanofiber layers did not affect the size selectivity of the membranes (Figure 3). Molecular-weight cutoff (MWCO)

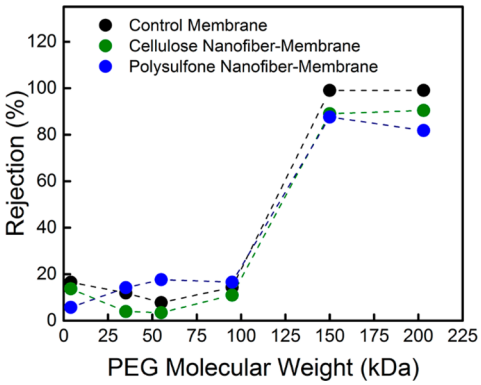

Figure 3. PEG rejection as a function of molecular weight for the control membranes, cellulose nanofiber-membranes, and polysulfone nanofiber-membranes.

values were determined using PEG solutions with increasing molecular weights. The cellulose nanofiber-membranes, polysulfone nanofiber-membranes, and control membranes had MWCOs greater than 95 kDa, which is consistent with the values previously reported by Millipore.[52] Nanofiber layers have porosities greater than 80%[53] and calculated intrafiber spacings of 3 μm.[54] Our retained MWCO data suggest that the small membrane pores (18.0 ± 8 nm) remained accessible and continued to control the size selectivity of the membranes. Additionally, the retained rejection values indicate that PEG did not adhere to the nanofiber layers, potentially because of the short contact time during membrane operation (as discussed in section 3.6). Notably, previous surface modifications of membranes, including the addition of silver nanoparticles (<5 nm)[6] and a polydopamine surface coating (1−30 nm),[55] decreased the size of the surface pores, which adversely impacted membrane performance, including altering membrane rejection and pure-water flux.

3.4. Pure-Water Flux of Cellulose Nanofiber-Membranes and Polysulfone Nanofiber-Membranes. The pure-water fluxes of free-standing cellulose and polysulfone nanofiber layers (no ultrafiltration membranes) were determined to be 37000 and 40000 L m^{-2} h^{-1}, respectively. The high fluxes of the porous nanofibers are consistent with the literature[56] and 2 orders of magnitude greater than the flux of the control ultrafiltration membranes (400 L m^{-2} h^{-1}) at the same applied pressure of 0.14 bar. These results indicate that free-standing nanofiber layers have very high flux values that should not impede the fluxes of ultrafiltration membranes and that such layers are able to withstand low TMPs. We next tested the cellulose nanofiber-membranes and polysulfone nanofiber-membranes at multiple TMPs (from 0.5 to 4.5 bar) and in a cross-flow configuration relevant to ultrafiltration operation.

Figure 4 displays the compaction curves (flux as a function of time) acquired using a cross-flow configuration at 1.5 and 3.5 bar for the cellulose nanofiber-membranes, polysulfone nanofiber-membranes, and control membranes. In commercial

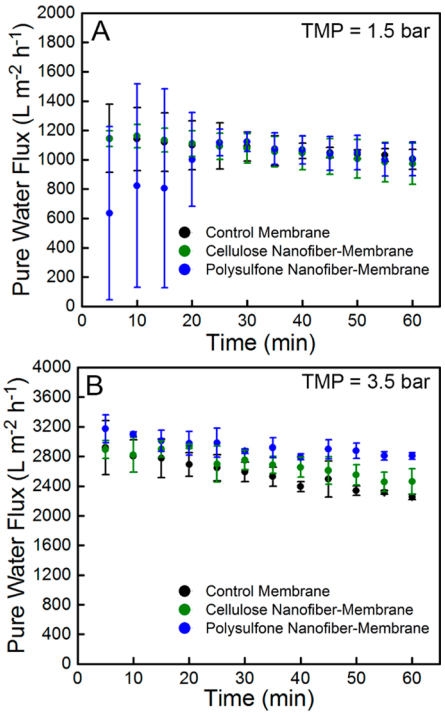

Figure 4. Compaction curves for the control membranes, cellulose nanofiber-membranes, and polysulfone nanofiber-membranes at TMP values of (A) 1.5 and (B) 3.5 bar. Error bars denote standard deviations.

ultrafiltration processes, the flow of the feed is tangential to the membrane surface. Therefore, we wanted to ensure that the nanofiber layer could withstand relevant operational conditions. The compaction curve for the cellulose nanofiber-membranes displays the same behavior as the compaction curve for the control membranes at both low and high TMP values. Potentially because of the hydrophilicity of the cellulose nanofiber layer, water was encouraged to flow through the nanofibers with minimal resistance. In contrast, the flux of the polysulfone nanofiber-membranes increased for the first 25 min of testing at a TMP of 1.5 bar before displaying the same gradual reduction in flux displayed by the cellulose nanofiber-membranes and control membranes. The slower compaction behavior occurred despite the prewetting procedure, which has been reported to aid in displacing trapped air from within the void space of nanofibers.[19] The initial reduced membrane flux could be due to the challenge of wetting the hydrophobic surface of the nanofibers in a cross-flow configuration wherein much of the feedwater does not penetrate into the nanofiber layer.[57] At the higher TMP of 3.5 bar, a greater driving force might have induced contact between the water molecules and the nanofiber layer; the compaction curves for the cellulose nanofiber-membranes and polysulfone nanofiber-membranes are consistent with the compaction curve for the control membranes.

To determine the appropriate pressure range for operating membranes, the membrane flux can be tested as a function of applied pressure. Figure 5 suggests that the pure-water flux of the nanofiber-enhanced membranes is affected by the applied pressure and the chemistry of the nanofiber layer. From 0.5 to 4.5 bar, a linear relationship was observed between flux and TMP for the polysulfone nanofiber-membranes and the control membranes, as expected in membrane technology. However,

DOI: 10.1021/acs.iecr.7b00631
Ind. Eng. Chem. Res. 2017, 56, 5724−5733

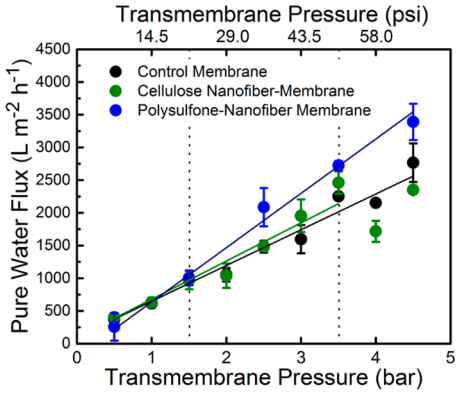

Figure 5. Pure-water fluxes of the control membranes, cellulose nanofiber-membranes, and polysulfone nanofiber-membranes as functions of transmembrane pressure (TMP). The solid lines represent the fits used to calculate hydraulic permeance. Error bars denote standard deviations.

the cellulose nanofiber-membranes exhibited a linear trend only when tested using TMPs ranging from 0.5 to 3.5 bar. Using the data from these linear regimes, the pure-water hydraulic permeance (or the increase in total membrane throughput per unit operating pressure) was determined using the individual error for each data point. The statistical significance of the linear regressions was determined using a modified *z*-test.[44] The control membranes, cellulose nanofiber-membranes, and polysulfone nanofiber-membranes exhibited cross-flow permeances of 560, 580, and 830 L m^{-2} h^{-1} bar^{-1}, respectively. Taking into account the differences in membrane thicknesses, the hydraulic permeabilities were determined to be 56, 185, and 158 L m^{-2} h^{-1} bar^{-1} mm^{-1} for the control membranes, cellulose nanofiber-membranes, and polysulfone nanofiber-membranes, respectively. The polysulfone nanofiber-membranes had a statistically higher permeance than the control membranes. Furthermore, at a TMP of 3.5 bar, the polysulfone nanofiber-membrane had a 35% higher flux than the control membrane.

Taking a closer look at the flux behaviors of the cellulose nanofiber-membranes, polysulfone nanofiber-membranes, and control membranes, at low TMP values (0.5−1.5 bar), the pure-water flux persisted upon the addition of a nanofiber layer (Figure 5). Within this low TMP range, the permeation of water was not impeded, possibly because of the inherent porosity and high flux of the nanofiber layer. Our results contrast those reported in the literature, wherein the addition of polymers, nanoparticles, and polymer thin films to the surface of ultrafiltration membranes decreased the membrane flux.[6,31,48−50] For example, coils of cellulose derivatives on the surface of membranes reduced the flux by 30% because the coils blocked and/or reduced the size of the pores.[58] Furthermore, the persistence of flux is notable, as the new top layer of electrospun nanofibers was 50 μm thick whereas the other ultrafiltration membrane surface modifications were nanometer-scale (50 and 4 nm).[6,40] Notably, we did not chemically tether the nanofiber layers to the membranes, and thus, the selective surface pores remained available and undamaged to control membrane throughput.

At TMP values between 1.5 and 3.5 bar, the polysulfone nanofiber-membranes, cellulose nanofiber-membranes, and control membranes exhibited a linear relationship between the pure-water flux and TMP, indicating that operation is feasible within this pressure regime for all of these membranes. The cellulose nanofiber-membranes exhibited a permeance that was statistically the same as that of the control membranes, whereas the permeance of the polysulfone nanofiber-membranes was greater than that of the control membranes. Above a TMP of 3.5 bar, differences in the flux behavior emerged among the cellulose nanofiber-membranes, polysulfone nanofiber-membranes, and control membranes. A linear relationship between flux and TMP for the cellulose nanofiber-membrane was no longer observed, whereas for the polysulfone nanofiber-membranes and control membranes, the pure-water flux increased linearly across all TMP values tested.

We hypothesize that the differing elongation properties of the nanofiber layer might influence their ability to withstand the forces induced by cross-flow during membrane operation. The dry tensile strengths and Young's moduli for polysulfone and cellulose nanofibers have been reported to be similar.[59,60] Interestingly, the elongation of natural cellulose fibers is known to increase with wetting,[61] which contrasts the phenomena typically observed when synthetic fibers are wetted. When hydrated during normal cross-flow conditions, the cellulose nanofibers potentially elongate and, thus, vibrate or move more than the polysulfone nanofibers. Additionally, the junction points within the randomly accumulated polysulfone nanofiber layer are likely to be stronger than those in the cellulose nanofiber layer because, during the electrospinning process, polysulfone interacts with water vapor as a nonsolvent, thus enhancing the interconnected nature of the polysulfone fibers.[62]

The random accumulation of fibers within the nanofiber layer might also be related to the increased membrane flux exhibited by the polysulfone nanofiber-membranes. The nanofiber layer has individual fibers located at various distances from the membrane active surface. Ma and Song determined the impact of spacer configuration on the flux of reverse-osmosis membranes.[63] Simulations compared filament spacers arranged in a "zigzag" configuration to those arranged in a "cavity configuration", where both configurations placed filaments at 4-mm intervals. In the zigzag configuration, filaments had alternating *z*-axis distances (0 and 0.55 mm) relative to the surface of the membrane; in the cavity configuration, filaments were fixed on the membrane's surface (*z*-axis distance = 0 mm). The zigzag configuration outperformed the cavity configuration. Won et al. also reported that having filaments at different *z*-axis locations increased solution velocity at the membrane surface and decreased concentration polarization.[64] Potentially because our randomly oriented nanofibers have varying *z*-axis distances, they might enhance water transport using a mechanism similar to that reported by Ma and Song. In our experiments, enhancement is most apparent with a robust nanofiber chemistry that can withstand desirable TMPs and preserve the zigzag configuration.

3.5. Morphologies of Cellulose Nanofiber-Membranes and Polysulfone Nanofiber-Membranes after Flux Testing. Digital images and SEM micrographs were acquired to qualitatively assess the conditions of the cellulose nanofiber-membranes, polysulfone nanofiber-membranes, and control membranes after flux testing at a TMP of 3.5 bar (Figure 6). The digital images do not show any visual defects within the membrane active area. Additionally, the random fiber orientations of the cellulose and polysulfone nanofiber layers were retained, as shown in the SEM micrographs. As discussed

DOI: 10.1021/acs.iecr.7b00631
Ind. Eng. Chem. Res. 2017, 56, 5724−5733

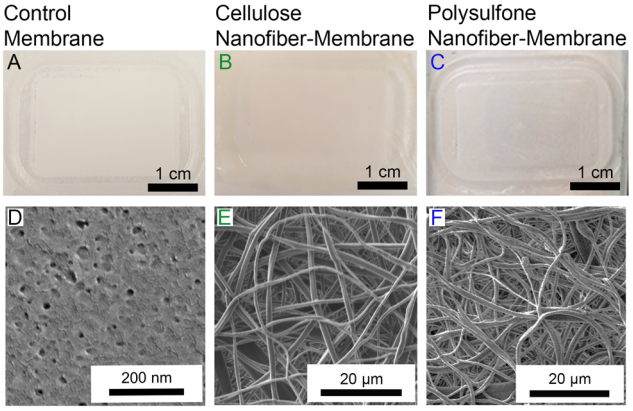

Figure 6. Digital images and SEM micrographs of the (A,D) control membranes, (B,E) cellulose nanofiber-membranes, and (C,F) polysulfone nanofiber-membranes after flux testing at a TMP of 3.5 bar.

previously, at higher TMPs, the individual cellulose nanofibers within the randomly accumulated layer might be shifting while in flow. However, microscopy revealed that cross-flow testing at a TMP of 3.5 bar did not break or damage the nanofibers, indicating that they were robust enough to withstand the forces induced during membrane operation. After the flux testing, we removed the cellulose and polysulfone nanofiber layers and determined that the average pore diameter (17.0 ± 8 nm) and pore coverage (6.4% ± 0.2%) remained consistent with those of the as-received control membranes (Figure S4 of the Supporting Information). The nanofiber layers did not alter the base ultrafiltration membranes, reinforcing our finding that all membranes tested in this work exhibited the same MWCO (Figure 4).

3.6. Protein Fouling Resistances of the Cellulose Nanofiber-Membrane and Polysulfone Nanofiber-Membranes. When evaluated using a dead-end stirred cell, the cellulose nanofiber-membranes and polysulfone nanofiber-membranes exhibited improved fouling resistance compared to the control membranes (Figure 7). The amount of BSA retained by the cellulose nanofiber-membranes (12 ± 5 μg cm^{-2}) and polysulfone nanofiber-membranes (15 ± 9 μg cm^{-2}) were statistically lower than the amounts retained by the control membranes (212 ± 20 μg cm^{-2}), indicating that the nanofiber layers mitigated fouling. It has previously been suggested that randomly orientated fibers can induce shear stresses that can prevent the attachment of BSA to membranes.[65] This is consistent with the work of Fan et al., who reported that short polyaniline nanofibers (259 nm length × 43 nm diameter) on the membrane surface decreased BSA fouling.[66] Furthermore, when the BSA fouling tests were conducted on cellulose nanofiber-membranes and polysulfone nanofiber-membranes, equal quantities of solution passed through the nanofiber-enhanced membranes in one-half the amount of time it took to pass through the control membranes. With the addition of the nanofiber layer, the BSA had less time in contact with the surface of the membranes. In our studies, fouling resistance was improved by both nanofiber layer chemistries, indicating that nanofiber morphology is more important than nanofiber chemistry in enhancing the fouling resistance performance of ultrafiltration membranes in operation.

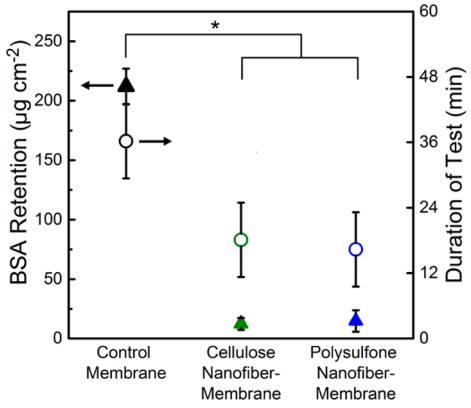

Figure 7. Protein resistance of the control membranes, cellulose nanofiber-membranes, and polysulfone nanofiber-membranes. BSA retention (solid triangles) refers to the left axis, and duration of test (open circles) refers to the right axis. Experiments were conducted using a dead-end stirred cell. Error bars denote standard deviation, and one asterisk (*) denotes a $p \leq 0.05$ significance between samples.

Table 1 indicates that, when the residence time between the nanofibers (no membranes) and the BSA protein was increased to 1 h, fouling did indeed occur and chemistry plays a role. The cellulose nanofibers had a higher capacity for BSA adsorption than the polysulfone nanofibers. This is likely due to the hydroxyl groups of the cellulose interacting with the hydrophobic regions of the BSA.[67] The limited adsorption of BSA to the polysulfone nanofibers is consistent with BSA's reported chemical inertness. This supports our hypothesis that, because the nanofiber layer increased the membrane flux, there was a decrease in contact time between the protein and the nanofiber-enhanced membrane surface and thus, fouling decreased. The control membrane tests took 0.66 h compared to the nanofiber-enhanced membrane tests, which took 0.33 h to complete. This decrease in test duration is statistically different, and this shortened contact time might have contributed to the increased protein fouling resistance of the nanofiber-enhanced membranes over the control membranes. Further studies are needed to assess the long-term performance and flux restoration after cleaning of the nanofiber-enhanced membranes.

Table 1. Protein Adsorption by Free-Standing Cellulose Nanofibers and Polysulfone Nanofibers[a]

electrospun layer	adsorption of BSA (μg cm^{-2})
cellulose nanofibers	32 ± 10
polysulfone nanofibers	5 ± 2

[a]Test duration was 1 h for all samples.

4. CONCLUSIONS

This report demonstrates that electrospun nanofibers can effectively improve the performance of ultrafiltration membranes. Randomly accumulated, continuous, and cylindrical nanofibers with distinct chemistries but the same morphology were fabricated. With the addition of either cellulose or polysulfone nanofibers to an ultrafiltration membrane, selectivity remained the same; however, compaction time differed at low TMPs. The flux performance of the composite membranes diverged with increasing applied pressure. Independent of nanofiber chemistry, at lower TMP values,

DOI: 10.1021/acs.iecr.7b00631
Ind. Eng. Chem. Res. 2017, 56, 5724−5733

the flux of the nanofiber-enhanced membranes was the same as the control membranes. At TMP values above 3.5 bar, only the polysulfone nanofiber-membrane demonstrated a linear permeance relationship which may be attributed to the different elongation properties of polysulfone nanofibers compared to cellulose nanofibers. Polysulfone nanofiber-membranes had a 47% increase in permeance and a 35% increase in pure-water flux than the control ultrafiltration membranes at a TMP of 3.5 bar. The cellulose nanofiber-membranes and polysulfone nanofiber-membranes demonstrated a 90% improvement in fouling resistance over the control membranes, possibly because the presence of the nanofibers decreased the contact time between the protein and the membranes by 50%. For the first time, we have demonstrated that adding a nanofiber layer to an ultrafiltration membrane offers a rational approach to functionalizing a membrane without adversely impacting base membrane properties. We suggest that such composite membranes provide a new paradigm for further surface modifications, for instance, tailored delivery of antimicrobial agents.

■ ASSOCIATED CONTENT

Supporting Information

The Supporting Information is available and free of charge The Supporting Information is available free of charge on the ACS Publications website at DOI: 10.1021/acs.iecr.7b00631.

High-magnification SEM micrographs of nanofibers (Figure S1), FTIR spectra of nanofibers (Figure S2), compaction curves as a function of cellulose nanofiber layer thickness (50, 65, and 125 μm) on hand-cast ultrafiltration membranes (Figure S3), and SEM micrographs of membrane surfaces after flux testing (Figure S4) (PDF)

■ AUTHOR INFORMATION

Corresponding Author

*E-mail: schiffman@ecs.umass.edu. Tel.: 413-545-6143.

ORCID

Jessica D. Schiffman: 0000-0002-1265-5392

Notes

The authors declare no competing financial interest.

■ ACKNOWLEDGMENTS

This work was supported in part by a fellowship given by UMass to K.M.D. as part of the Biotechnology Training Program (NIH, National Research Service Award T32 GM108556). J.D.S. acknowledges the support of the National Science Foundation (NSF CBET-1342343 and NSF CBET-1719747). This work was partially supported by the Professor James M. Douglas Career Development Faculty Award and the U.S. Geological Survey State Water Resources Institute Program (USGS WRIP Grant 2015MA436B). Thanks are given to Dr. Alexander Ribbe, Dr. Michael Jercinovic, and Mr. Lou Raboin for guidance with SEM. We acknowledge the use of facilities at the W.M. Keck Center for Electron Microscopy.

■ ABBREVIATIONS

BSA = bovine serum albumin
CL = cellulose
DI = deionized
DMF = dimethylformamide
THF = tetrahydrofuran
MWCO = molecular-weight cutoff
PEG = polyethylene glycol
PSf = polysulfone
SEM = scanning electron microscopy
TMP = transmembrane pressure

■ REFERENCES

(1) Lin, C.-E.; Wang, J.; Zhou, M.-Y.; Zhu, B.-K.; Zhu, L.-P.; Gao, C.-J. Poly(*m*-phenylene isophthalamide) (PMIA): A Potential Polymer for Breaking through the Selectivity-Permeability Trade-off for Ultrafiltration Membranes. *J. Membr. Sci.* **2016**, *518*, 72−78.

(2) Geise, G. M.; Lee, H.; Miller, D. J.; Freeman, B. D.; McGrath, J. E.; Paul, D. R. Water Purification by Membranes: The Role of Polymer Science. *J. Polym. Sci., Part B: Polym. Phys.* **2010**, *48*, 1685−1718.

(3) Gao, W.; Liang, H.; Ma, J.; Han, M.; Chen, Z.; Han, Z.; Li, G. Membrane Fouling Control in Ultrafiltration Technology for Drinking Water Production: A Review. *Desalination* **2011**, *272* (1−3), 1−8.

(4) Alzahrani, S.; Mohammad, A. W. Challenges and Trends in Membrane Technology Implementation for Produced Water Treatment: A Review. *J. Water Process Eng.* **2014**, *4*, 107−133.

(5) Kumar, R.; Isloor, A. M.; Ismail, A. F.; Rashid, S. A.; Matsuura, T. Polysulfone−Chitosan Blend Ultrafiltration Membranes: Preparation, Characterization, Permeation and Antifouling Properties. *RSC Adv.* **2013**, *3* (21), 7855.

(6) Mauter, M. S.; Wang, Y.; Okemgbo, K. C.; Osuji, C. O.; Giannelis, E. P.; Elimelech, M. Antifouling Ultrafiltration Membranes via Post-Fabrication Grafting of Biocidal Nanomaterials. *ACS Appl. Mater. Interfaces* **2011**, *3* (8), 2861−2868.

(7) Dobosz, K. M.; Kolewe, K. W.; Schiffman, J. D. Green Materials Science and Engineering Reduces Biofouling: Approaches for Medical and Membrane-Based Technologies. *Front. Microbiol.* **2015**, *6*, 196.

(8) Ding, Y.; Maruf, S.; Aghajani, M.; Greenberg, A. R. Surface Patterning of Polymeric Membranes and Its Effect on Antifouling Characteristics. *Sep. Sci. Technol.* **2017**, *52*, 240−257.

(9) Hoek, E. M. V.; Ghosh, A. K.; Huang, X.; Liong, M.; Zink, J. I. Physical−chemical Properties, Separation Performance, and Fouling Resistance of Mixed-Matrix Ultrafiltration Membranes. *Desalination* **2011**, *283*, 89−99.

(10) Ali, N.; Tari, S. S. M. Surface Modification of Polyethersulfone Ultrafiltration (PES-UF) Membrane Using Myoglobin as Modifying Agent. *Desalin. Water Treat.* **2012**, *47* (1−3), 171−181.

(11) Taurozzi, J. S.; Arul, H.; Bosak, V. Z.; Burban, A. F.; Voice, T. C.; Bruening, M. L.; Tarabara, V. V. Effect of Filler Incorporation Route on the Properties of Polysulfone−silver Nanocomposite Membranes of Different Porosities. *J. Membr. Sci.* **2008**, *325* (1), 58−68.

(12) Luo, C. J.; Stoyanov, S. D.; Stride, E.; Pelan, E.; Edirisinghe, M. Electrospinning versus Fibre Production Methods: From Specifics to Technological Convergence. *Chem. Soc. Rev.* **2012**, *41* (13), 4708−4735.

(13) Ghasemi-Mobarakeh, L.; Semnani, D.; Morshed, M. A Novel Method for Porosity Measurement of Various Surface Layers of Nanofibers Mat Using Image Analysis for Tissue Engineering Applications. *J. Appl. Polym. Sci.* **2007**, *106* (4), 2536−2542.

(14) Feng, C.; Khulbe, K. C.; Matsuura, T.; Tabe, S.; Ismail, A. F. Preparation and Characterization of Electro-Spun Nanofiber Membranes and Their Possible Applications in Water Treatment. *Sep. Purif. Technol.* **2013**, *102*, 118−135.

(15) Homaeigohar, S. S.; Buhr, K.; Ebert, K. Polyethersulfone Electrospun Nanofibrous Composite Membrane for Liquid Filtration. *J. Membr. Sci.* **2010**, *365* (1−2), 68−77.

(16) Gopal, R.; Kaur, S.; Feng, C. Y.; Chan, C.; Ramakrishna, S.; Tabe, S.; Matsuura, T. Electrospun Nanofibrous Polysulfone Membranes as Pre-Filters: Particulate Removal. *J. Membr. Sci.* **2007**, *289* (1−2), 210−219.

DOI: 10.1021/acs.iecr.7b00631
Ind. Eng. Chem. Res. 2017, 56, 5724−5733

(17) Hardick, O.; Dods, S.; Stevens, B.; Bracewell, D. G. Nanofiber Adsorbents for High Productivity Continuous Downstream Processing. *J. Biotechnol.* **2015**, *213*, 74−82.
(18) Ma, H.; Hsiao, B. S.; Chu, B. Functionalized Electrospun Nanofibrous Microfiltration Membranes for Removal of Bacteria and Viruses. *J. Membr. Sci.* **2014**, *452*, 446−452.
(19) Hoover, L. A.; Schiffman, J. D.; Elimelech, M. Nanofibers in Thin-Film Composite Membrane Support Layers: Enabling Expanded Application of Forward and Pressure Retarded Osmosis. *Desalination* **2013**, *308*, 73−81.
(20) Nair, A. K.; Shalin, P. M.; JagadeeshBabu, P. E. Performance Enhancement of Polysulfone Ultrafiltration Membrane Using TiO2 Nanofibers. *Desalin. Water Treat.* **2016**, *57* (23), 10506−10514.
(21) Fan, Z.; Wang, Z.; Sun, N.; Wang, J.; Wang, S. Performance Improvement of Polysulfone Ultrafiltration Membrane by Blending with Polyaniline Nanofibers. *J. Membr. Sci.* **2008**, *320* (1), 363−371.
(22) Dolina, J.; Jiříček, T.; Lederer, T. Membrane Modification with Nanofiber Structures Containing Silver. *Ind. Eng. Chem. Res.* **2013**, *52* (39), 13971−13978.
(23) Dolina, J.; Jiříček, T.; Lederer, T. Biocide Modification of Ultrafiltration Membranes Using Nanofiber Structures. *Desalin. Water Treat.* **2015**, *56* (12), 3252−3258.
(24) Bai, H.; Wang, X.; Sun, H.; Zhang, L. Permeability and Morphology Study of Polysulfone Composite Membrane Blended with Nanocrystalline Cellulose. *Desalin. Water Treat.* **2015**, *53* (11), 2882−2896.
(25) Liu, H.; Hsieh, Y.-L. Ultrafine Fibrous Cellulose Membranes from Electrospinning of Cellulose Acetate. *J. Polym. Sci., Part B: Polym. Phys.* **2002**, *40* (18), 2119−2129.
(26) Frey, M. W. Electrospinning Cellulose and Cellulose Derivatives. *Polym. Rev.* **2008**, *48* (2), 378−391.
(27) Kumar, R.; Isloor, A. M.; Ismail, A. F. Preparation and Evaluation of Heavy Metal Rejection Properties of Polysulfone/chitosan, polysulfone/N-Succinyl Chitosan and polysulfone/N-Propylphosphonyl Chitosan Blend Ultrafiltration Membranes. *Desalination* **2014**, *350*, 102−108.
(28) Rieger, K. A.; Cho, H. J.; Yeung, H. F.; Fan, W.; Schiffman, J. D. Antimicrobial Activity of Silver Ions Released from Zeolites Immobilized on Cellulose Nanofiber Mats. *ACS Appl. Mater. Interfaces* **2016**, *8* (5), 3032−3040.
(29) Ma, Z.; Kotaki, M.; Ramakrishna, S. Electrospun Cellulose Nanofiber as Affinity Membrane. *J. Membr. Sci.* **2005**, *265* (1−2), 115−123.
(30) Yip, N. Y.; Tiraferri, A.; Phillip, W. A.; Schiffman, J. D.; Elimelech, M. High Performance Thin-Film Composite Forward Osmosis Membrane. *Environ. Sci. Technol.* **2010**, *44* (10), 3812−3818.
(31) Senbil, N.; He, W.; Démery, V.; Dinsmore, A. D. Effect of Interface Shape on Advancing and Receding Fluid-Contact Angles around Spherical Particles. *Soft Matter* **2015**, *11*, 4999−5003.
(32) Phillip, W. A.; Amendt, M.; O'Neill, B.; Chen, L.; Hillmyer, M. A.; Cussler, E. L. Diffusion and Flow across Nanoporous Polydicyclopentadiene-Based Membranes. *ACS Appl. Mater. Interfaces* **2009**, *1* (2), 472−480.
(33) Dornath, P.; Cho, H. J.; Paulsen, A. D.; Dauenhauer, P. J.; Fan, W. Highly Efficient Mechano-Catalytic Depolymerization of Crystalline Cellulose by Formation of Branched Glucan Chains. *Green Chem.* **2015**, *17* (2), 769−775.
(34) Reddy, A. V. R.; Mohan, D. J.; Bhattacharya, A.; Shah, V. J.; Ghosh, P. K. Surface Modification of Ultrafiltration Membranes by Preadsorption of a Negatively Charged Polymer. *J. Membr. Sci.* **2003**, *214* (2), 211−221.
(35) Asatekin, A.; Kang, S.; Elimelech, M.; Mayes, A. M. Anti-Fouling Ultrafiltration Membranes Containing Polyacrylonitrile-*graft*-poly(ethylene oxide) Comb Copolymer Additives. *J. Membr. Sci.* **2007**, *298* (1−2), 136−146.
(36) Susanto, H.; Arafat, H.; Janssen, E. M. L.; Ulbricht, M. Ultrafiltration of Polysaccharide−Protein Mixtures: Elucidation of Fouling Mechanisms and Fouling Control by Membrane Surface Modification. *Sep. Purif. Technol.* **2008**, *63* (3), 558−565.
(37) Teella, A.; Huber, G. W.; Ford, D. M. Separation of Acetic Acid from the Aqueous Fraction of Fast Pyrolysis Bio-Oils Using Nanofiltration and Reverse Osmosis Membranes. *J. Membr. Sci.* **2011**, *378* (1−2), 495−502.
(38) Eren, E.; Sarihan, A.; Eren, B.; Gumus, H.; Kocak, F. O. Preparation, Characterization and Performance Enhancement of Polysulfone Ultrafiltration Membrane Using PBI as Hydrophilic Modifier. *J. Membr. Sci.* **2015**, *475*, 1−8.
(39) Fan, Z.; Wang, Z.; Sun, N.; Wang, J.; Wang, S. Performance Improvement of Polysulfone Ultrafiltration Membrane by Blending with Polyaniline Nanofibers. *J. Membr. Sci.* **2008**, *320* (1−2), 363−371.
(40) Moghimifar, V.; Raisi, A.; Aroujalian, A. Surface Modification of Polyethersulfone Ultrafiltration Membranes by Corona Plasma-Assisted Coating TiO_2 Nanoparticles. *J. Membr. Sci.* **2014**, *461*, 69−80.
(41) Kasemset, S.; Lee, A.; Miller, D. J.; Freeman, B. D.; Sharma, M. M. Effect of Polydopamine Deposition Conditions on Fouling Resistance, Physical Properties, and Permeation Properties of Reverse Osmosis Membranes in Oil/Water Separation. *J. Membr. Sci.* **2013**, *425−426*, 208−216.
(42) Kolewe, K. W.; Dobosz, K. M.; Rieger, K. A.; Chang, C.-C.; Emrick, T.; Schiffman, J. D. Antifouling Electrospun Nanofiber Mats Functionalized with Polymer Zwitterions. *ACS Appl. Mater. Interfaces* **2016**, *8* (41), 27585−27593.
(43) Rieger, K.; Thyagarajan, R.; Hoen, M.; Yeung, H.; Ford, D.; Schiffman, J. Transport of Microorganisms into Cellulose Nanofiber Mats. *RSC Adv.* **2016**, *6* (29), 24438−24445.
(44) Paternoster, R.; Brame, R.; Mazerolle, P.; Piquero, A. Using the Correct Statistical Test for the Equality of Regression Coefficients. *Criminology* **1998**, *36* (4), 859−866.
(45) Ma, Z.; Ramakrishna, S. Electrospun Regenerated Cellulose Nanofiber Affinity Membrane Functionalized with Protein A/G for IgG Purification. *J. Membr. Sci.* **2008**, *319* (1−2), 23−28.
(46) Schiffman, J. D.; Elimelech, M. Antibacterial Activity of Electrospun Polymer Mats with Incorporated Narrow Diameter Single-Walled Carbon Nanotubes. *ACS Appl. Mater. Interfaces* **2011**, *3* (2), 462−468.
(47) Wang, Z.-G.; Wang, J.-Q.; Xu, Z.-K. Immobilization of Lipase from Candida Rugosa on Electrospun Polysulfone Nanofibrous Membranes by Adsorption. *J. Mol. Catal. B: Enzym.* **2006**, *42* (1−2), 45−51.
(48) Yao, Y.; Zhu, P.; Ye, H.; Niu, A.; Gao, X.; Wu, D. Polysulfone Nanofibers Prepared by Electrospinning and Gas/jet-Electrospinning. *Front. Chem. China* **2006**, *1* (3), 334−339.
(49) Shurvell, H. F.; Southby, M. C. Infrared and Raman Spectra of Tetrahydrofuran Hydroperoxide. *Vib. Spectrosc.* **1997**, *15* (1), 137−146.
(50) Jonoobi, M.; Harun, J.; Mathew, A. P.; Hussein, M. Z. B.; Oksman, K. Preparation of Cellulose Nanofibers with Hydrophobic Surface Characteristics. *Cellulose* **2010**, *17* (2), 299−307.
(51) Bormashenko, E.; Pogreb, R.; Whyman, G.; Bormashenko, Y.; Jager, R.; Stein, T.; Schechter, A.; Aurbach, D. The Reversible Giant Change in the Contact Angle on the Polysulfone and Polyethersulfone Films Exposed to UV Irradiation. *Langmuir* **2008**, *24* (12), 5977−5980.
(52) *Biomax Membranes: The Membrane of Choice for Fast Processing and Exceptional Chemical Resistance*; EMD Millipore: Billerica, MA, 2015.
(53) Moghadam, B. H.; Haghi, A. K.; Kasaei, S.; Hasanzadeh, M. Computational-Based Approach for Predicting Porosity of Electrospun Nanofiber Mats Using Response Surface Methodology and Artificial Neural Network Methods. *J. Macromol. Sci., Part B: Phys.* **2015**, *54* (11), 1404−1425.
(54) Ma, H.; Burger, C.; Hsiao, B. S.; Chu, B. Ultra-Fine Cellulose Nanofibers: New Nano-Scale Materials for Water Purification. *J. Mater. Chem.* **2011**, *21* (21), 7507.
(55) McCloskey, B. D.; Park, H. B.; Ju, H.; Rowe, B. W.; Miller, D. J.; Freeman, B. D. A Bioinspired Fouling-Resistant Surface Modification for Water Purification Membranes. *J. Membr. Sci.* **2012**, *413−414*, 82−90.

DOI: 10.1021/acs.iecr.7b00631
Ind. Eng. Chem. Res. 2017, 56, 5724−5733

(56) Huang, L.; Arena, J. T.; Manickam, S. S.; Jiang, X.; Willis, B. G.; McCutcheon, J. R. Improved Mechanical Properties and Hydrophilicity of Electrospun Nanofiber Membranes for Filtration Applications by Dopamine Modification. *J. Membr. Sci.* **2014**, *460*, 241−249.
(57) Kochan, J.; Wintgens, T.; Hochstrat, R.; Melin, T. Impact of Wetting Agents on the Filtration Performance of Polymeric Ultrafiltration Membranes. *Desalination* **2009**, *241* (1−3), 34−42.
(58) Beeskow, T. C.; Kusharyoto, W.; Anspach, F. B.; Kroner, K. H.; Deckwer, W.-D. Surface Modification of Microporous Polyamide Membranes with Hydroxyethyl Cellulose and Their Application as Affinity Membranes. *J. Chromatogr. A* **1995**, *715* (1), 49−65.
(59) Huang, L.; Manickam, S. S.; McCutcheon, J. R. Increasing Strength of Electrospun Nanofiber Membranes for Water Filtration Using Solvent Vapor. *J. Membr. Sci.* **2013**, *436*, 213−220.
(60) Dods, S. R.; Hardick, O.; Stevens, B.; Bracewell, D. G. Fabricating Electrospun Cellulose Nanofibre Adsorbents for Ion-Exchange Chromatography. *J. Chromatogr. A* **2015**, *1376*, 74−83.
(61) Miyake, H.; Gotoh, Y.; Ohkoshi, Y.; Nagura, M. Tensile Properties of Wet Cellulose. *Polym. J.* **2000**, *32* (1), 29−32.
(62) Tiraferri, A.; Yip, N. Y.; Phillip, W. A.; Schiffman, J. D.; Elimelech, M. Relating Performance of Thin-Film Composite Forward Osmosis Membranes to Support Layer Formation and Structure. *J. Membr. Sci.* **2011**, *367* (1−2), 340−352.
(63) Ma, S.; Song, L. Numerical Study on Permeate Flux Enhancement by Spacers in a Crossflow Reverse Osmosis Channel. *J. Membr. Sci.* **2006**, *284* (1−2), 102−109.
(64) Won, Y.-J.; Jung, S.-Y.; Jang, J.-H.; Lee, J.-W.; Chae, H.-R.; Choi, D.-C.; Hyun Ahn, K.; Lee, C.-H.; Park, P.-K. Correlation of Membrane Fouling with Topography of Patterned Membranes for Water Treatment. *J. Membr. Sci.* **2016**, *498*, 14−19.
(65) Jamshidi Gohari, R.; Lau, W. J.; Matsuura, T.; Ismail, A. F. Effect of Surface Pattern Formation on Membrane Fouling and Its Control in Phase Inversion Process. *J. Membr. Sci.* **2013**, *446*, 326−331.
(66) Fan, Z.; Wang, Z.; Duan, M.; Wang, J.; Wang, S. Preparation and Characterization of Polyaniline/Polysulfone Nanocomposite Ultrafiltration Membrane. *J. Membr. Sci.* **2008**, *310* (1−2), 402−408.
(67) Orelma, H.; Filpponen, I.; Johansson, L.-S.; Laine, J.; Rojas, O. J. Modification of Cellulose Films by Adsorption of CMC and Chitosan for Controlled Attachment of Biomolecules. *Biomacromolecules* **2011**, *12* (12), 4311−4318.

DOI: 10.1021/acs.iecr.7b00631
Ind. Eng. Chem. Res. 2017, 56, 5724−5733